Journal of Hazardous Materials 213–214 (2012) 387–392

Contents lists available at SciVerse ScienceDirect

Journal of Hazardous Materials

journal homepage: www.elsevier.com/locate/jhazmat

Immobilized smart RNA on graphene oxide nanosheets to specifically recognize and adsorb trace peptide toxins in drinking water

Xiangang Hu[a], Li Mu[b], Jianping Wen[b], Qixing Zhou[a,*]

[a] Key Laboratory of Pollution Processes and Environmental Criteria (Ministry of Education), College of Environmental Science and Engineering, Nankai University, Tianjin 300071, China
[b] Department of Biochemical Engineering, School of Chemical Engineering and Technology, Tianjin University, Tianjin 300072, China

ARTICLE INFO

Article history:
Received 24 October 2011
Received in revised form 14 January 2012
Accepted 6 February 2012
Available online 13 February 2012

Keywords:
Biological toxin contamination
Nanomaterial
Graphene oxide
Aptamer
Microcystin-LR

ABSTRACT

The contaminations of peptide toxins in drinking water lead directly to sickness and even death in both humans and animals. A smart RNA as aptamer is covalently immobilized on graphene oxide to form a polydispersed and stable RNA–graphene oxide nanosheet. RNA–graphene oxide nanosheets can resist nuclease and natural organic matter, and specifically adsorb trace peptide toxin (microcystin-LR) in drinking water. The adsorption data fit the pseudo-second-order kinetics and the Langmuir isotherm model. The adsorption capacity of RNA–graphene oxide nanosheets decreases at extreme pH, temperature, ionic strength and natural organic matter, but it is suitable to adsorb trance pollutants in contaminated drinking water. Compared with other chemical and biological sorbents, RNA–graphene oxide nanosheets present specific and competitive adsorption, and are easily synthesized and regenerated. Aptamer (RNA) covalently immobilized on graphene oxide nanosheets is a potentially useful tool in recognizing, enriching and separating small molecules and biomacromolecules in the purification of contaminated water and the preparation of samples.

1. Introduction

Cyanobacteria species vigorously produce toxic compounds, frequently referred to as cyanotoxins. These toxins are globally recognized as triggering health risks via sources of drinking water [1]. The high chemical stability and water solubility of cyanotoxins lead to a long persistence of contamination in sources of drinking water. The most prevalent of cyanotoxins is peptide microcystin-LR that has led to serious sicknesses and deaths in people and animals [1]. Recent studies have exhibited trace microcystin-LR (ng L^{-1} μg L^{-1}) in drinking water, and confirmed that very low concentrations (less than 1 μg L^{-1}) significantly interrupted cellular processes [2]. Therefore, an effective adsorbent is crucial for scientists to detect and remove trace microcystin-LR in drinking water.

Concern about the global occurrence of biological toxin contamination has prompted the development of adsorption and removal of toxins in drinking water. Recent advances in nanomaterials and biomaterials have attractive properties for the adsorption and removal of peptide toxins. Nanomaterials, such as silver and titanium dioxide nanoparticles, have been used to adsorb and remove microcystin-LR from water [3]. However, several challenges exist in the efficient application of nanomaterials, for example, aggregation, nonspecific adsorption, secondary contamination and toxicity [4]. In addition, adsorption onto geosorbents/coating by natural organic matter (NOM) reduces the efficiency of nanomaterials [5]. Biomaterials, such as bacteria and peat, were used to adsorb toxins in water [6,7], as well as there should be increased attention paid to secondary contamination and the efficiency at low concentrations (ng L^{-1}) on the adsorption using traditional biomaterials [8]. Antibodies or enzymes have been widely used to detect or adsorb peptide toxins by immunoassays and immunoaffinity [9]. Notably, the complex selection processes and tricky stability of antibodies and enzymes are the bottlenecks of the relevant application.

The above problems could be solved by aptamers. Aptamers, a new class of single-stranded DNA (ssDNA)/RNA molecules, are selected from synthetic nucleic acid libraries for molecular recognition [10–12]. The smart ssDNA/RNA can recognize various targets molecules, including proteins, nucleic acids, peptides, amino acids, cells, bacterial viruses, organics and small molecules [11,12]. In contrast to antibodies or enzymes, the smart ssDNA/RNA has the advantages of high affinity, specificity and stability with targets, and easy to prepare and modify at low cost [13]. The bare and supported ssDNA have been used to remove arsenide and mercury in water, respectively [14,15]. Furthermore, ssDNA was immobilized on sepharose particles to remove trace pharmaceuticals from drinking water [16]. It is known that ssDNA/RNA is unstable in the environment and easy to degrade by nuclease. The effects of NOM,

* Corresponding author. Tel.: +86 022 23507800; fax: +86 022 66229562.
E-mail address: zhouqx523@yahoo.com (Q. Zhou).

0304-3894/$ – see front matter © 2012 Elsevier B.V. All rights reserved.
doi:10.1016/j.jhazmat.2012.02.012

nuclease and other physicochemical conditions could pose serious challenges for the application of the smart ssDNA/RNA, which is still obscure.

Graphene oxide (GO) is a newly discovered nanomaterial possessing a large surface area (2630 $m^2\ g^{-1}$) with little toxicity, which is attractive to water purification [17–20]. Aptamer (ssDNA) noncovalently adsorbed on GO can resist DNase, but ssDNA releases from GO when it contacts targets [21]. Therefore, the noncovalent immobilzation of ssDNA/RNA is not a valid method against nuclease. In this work, smart RNA is covalently immobilized on GO nanosheets to enhance the stability of RNA, and then specifically adsorb trace (ng L^{-1}) microcystin-LR in drinking water. Two points are supposed for RNA–GO: (i) increasing the specific adsorption of GO nanosheets due to the smart RNA modification and (ii) enhancing the stability of RNA owing to the covalent immobilization on GO nanosheets. First, RNA–GO nanosheets are synthesized and then characterized using Fourier transform infrared spectra (FTIR) and atomic force microscopy (AFM) image, as well as the stability of RNA–GO against nuclease is explored by agarose gel electrophoresis. Subsequently, the capacity of recognition of RNA–GO is tested by specifically binding to the similar structure of peptide toxins. Furthermore, the adsorption characteristics and effects of physicochemical conditions (pH, temperature, ionic strength and NOM) are expounded. Finally, RNA–GO as a novel sorbent is compared with other chemical and biological materials.

2. Materials and methods

2.1. Materials

The aptamer (RNA) specifically binding to microcystin-LR was originally selected from a random RNA pool (6×10^{14}) by Gu and Famulok [22]. The sequence is described as the following: 5′-***GGGAGAGACAAGCUUGGGUC***CCGGGGUAGGGAUGGGAGGUAUGGAGGGGUCCUUGUUUCC***CUCUUGCUCUUCCUAGGAGU***-3′

The first and last 20 bases are the primers for the RNA selection, as the italic characters. The two ends of a random RNA have the same sequence as the smart RNA. The middle 40 bases of the random RNA sequence are set with the same amount and percentage of bases as the smart RNA. The sequence of the random RNA is written as:

5′-***GGGAGAGACAAGCUUGGGU***CGCGUGGAGUGGAGGUGAGGAUGCGAGUGCGUGUCUUGUC***CUCUUGCUCUUCCUAGGAGU***-3′

The both RNA sequences were modified using 5′-amino groups with 6 carbon stems, and synthesized in Sigma Genosys. Four peptide toxins (microcystin-LR, microcystin-RR, microcystin-LW and nodularin) with similar structures, RNase I and other chemical agents are from Sigma–Aldrich (analytical standard or more purity). Suwannee River Humic Acid (SRHA) was purchased from the International Humic Substances Society. The purity water was achieved from Milli-Q water (18.2 MΩ).

2.2. Synthesis of RNA–GO nanosheets

GO was synthesized from natural graphite powder (45 μm, Sigma–Aldrich) using a modified Hummers method [17,18]. Briefly, 2 g graphite powder was ground with 100 g NaCl to reduce the particle size. H_2SO_4 (98%, 80 mL) and $KMnO_4$ (15 g) were slowly added under cooling ice and stirred for 2 h. Afterwards, the mixture was stirred at 40 °C for 2 h. Successively, water (180 mL) and 30% H_2O_2 solution (20 mL) were added and stirred for 3 h. The mixture was washed by repeated centrifugation and filtration, first with 5% HCl, and then with purified water. To confirm the removal of inorganic ions, atomic absorption spectrometry and Ba^{2+} was used to detect the residue of metal ions and SO_4^{2-} in the rinsed solution, respectively. There were no detected metal ions and SO_4^{2-} in the final rinsed solution after repeated wash, centrifugation and filtration. The suspension was dried at 60 °C for 24 h to obtain GO powder.

Epoxy, hydroxyl, carbonyl and carboxyl have been shown to exist in GO [23]. For the subsequent immobilization of RNA, more carboxylic groups are preferred in GO. The method of conversion hydroxyl groups into carboxylic groups was based on a previous work [24]. GO aqueous suspension (2 mg mL^{-1}) was sonicated for 1 h to achieve a homogeneous suspension. NaOH (1.5 g) and chloroacetic acid (1.0 g) were added to 5 mL GO suspension and then sonicated for 12 h to form carboxylic groups on GO.

To immobilize RNA on GO, the carboxylic groups of GO (0.2 mg mL^{-1}) were activated with 1-ethyl-3-(3-dimethylaminopropyl)-carbodiimide (0.2 M) and N-hydroxysulfosuccinimide (0.5 M) for 1 h. After a rinse with water, RNA (0.5 mg) was added into 1 mL GO suspension incubated overnight for grafting. At the end of the incubation, RNA–GO was rinsed thoroughly with phosphate buffered saline (pH 7.4) to remove unbound RNA. Finally, RNA–GO was filtrated (10 kDa) and lyophilized. The schematic illustration of the fabrication process of RNA–GO nanosheets is presented in Fig. 1.

2.3. Adsorption tests and analytical methods

Adsorption tests were conducted in 50 mL vial with drinking water. The drinking water without the tested toxins was taken directly from tap water. To confirm the specific adsorption, the random RNA–GO (0.2 mg), the smart RNA–GO (0.2 mg) and bare GO (0.2 mg) were incubated with 500 ng L^{-1} toxins (microcystin-LR, microcystin-RR, microcystin-LW and nodularin), respectively. To test the competitive adsorption, the effect of SRHA (2 and 20 mg L^{-1}) as standard NOM on adsorption was studied. For adsorption kinetics test, the smart RNA–GO with microcystin-LR (500 ng L^{-1}) was shaken at 100 rpm at 25 °C for 10–120 min. For adsorption isotherms test, the smart RNA–GO with microcystin-LR (50–2000 ng L^{-1}) was shaken for 100 min at 100 rpm and 25 °C. The adsorption equilibrium time was based on the results of adsorption

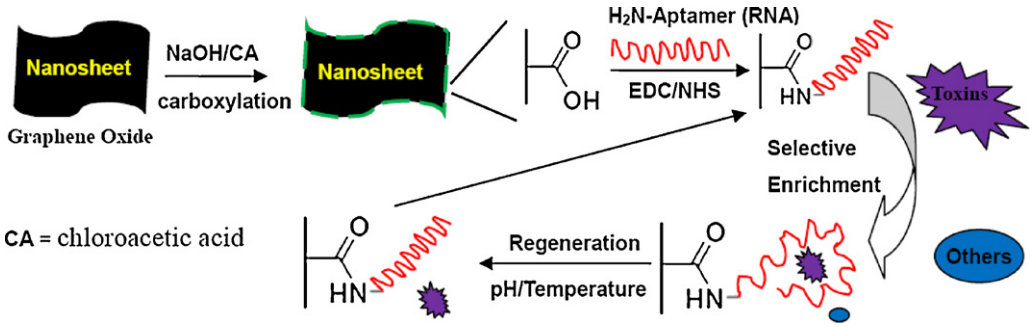

Fig. 1. Schematic fabrication process of RNA–graphene oxide nanosheets. Oxygen and hydroxyl groups can be located randomly above and/or below graphene oxide. Most of carboxyl groups are located on the edge of graphene oxide.

kinetics. The above spiked concentrations were comparable with the concentrations of actual contaminated drinking water [1,2].

A separate set of experiments were conducted to study the effects of pH (adjusted with NaOH and HCl from 5 to 9), temperature (10–50 °C) and ionic strength (1 mM NaCl and 1 M NaCl) on the adsorption in water. For the ionic strength test only, NaCl was spiked in pure water. The other experiments were conducted in natural drinking water. Afterward, the samples were centrifuged at 2500 × *g* for 15 min, and RNA–GO was taken out. The concentration of toxins in the solution was analyzed. Before detection, 50 mL sample was concentrated into 0.2 mL by solid phase extraction (Waters, 500 mg, HLB). The concentrations of microcystin-LR, microcystin-RR, microcystin-LW and nodularin were detected using high performance liquid chromatography tandem mass spectrometry [1]. Limits of quantitation (LOQs) were 0.5–1 ng L^{-1} in the water before concentration for different toxins. The recoveries were 88 ± 3% at the concentrations of 5 and 50 ng L^{-1} toxins in 50 mL drinking water.

2.4. Adsorption models

The adsorption kinetics data were fitted by pseudo-first and second-order kinetic models as expressed by the following equations, respectively.

$$\log\ (q_e - q_t) = \log\ q_e - \frac{k_1}{2.303}t \quad (1)$$

$$\frac{dq_1}{dt} = k_2(q_{eq} - q_t)^2 \quad (2)$$

where q_{eq} represents the sorption capacity (ng mg^{-1}) at equilibrium and q_t represents the amount (ng mg^{-1}) of adsorption at time t (min). k_1 (min^{-1}) and k_2 (mg ng^{-1} min^{-1}) represent the pseudo-first and second-order rate constants, respectively. The data of adsorption isotherms were fitted using Langmuir (Eq. (3)) and Freundlich isotherm (Eq. (4)) models written as the following:

$$q_{eq} = \frac{bQ_{max} - C_{eq}}{1 + bC_{eq}} \quad (3)$$

$$q_{eq} = KC_{eq}^{1/n} \quad (4)$$

where Q_{max} (ng mg^{-1}) represents the maximum adsorption capacity; C_{eq} represents the equilibrium toxin concentration (ng L^{-1}); q_{eq} (ng mg^{-1}) represents the equilibrium amount of toxins on sorbent; b represents the equilibrium constant related to the energy of sorption; K and n represent the empirical constants.

3. Results and discussion

3.1. Characteristics of GO and RNA–GO nanosheets

FTIR, AFM and agarose gel electrophoresis were used to expound the characteristics of GO and RNA–GO, as shown in Fig. 2. FTIR was to identify the functional groups attached on GO and RNA–GO, as described in Fig. 2a. GO exhibited a strong band at 1, 750 cm^{-1} assigned to the C=O stretching vibrations from carbonyl and carboxyl groups. The band at 1200 cm^{-1} assigned to the C—OH stretching vibrations was not obvious due to the modification of NaOH and chloroacetic acid. The spectrum of GO has a carboxyl (C=O) stretching peak at around 1750 cm^{-1}, but after the modification with RNA the peak shifted to 1640 cm^{-1}, which represented the amide carbonyl-stretching mode. In addition, at 1120 and 1218 cm^{-1}, RNA backbone and bases (C=O) were evident. FTIR proved that RNA was covalently immobilized on GO via the amide

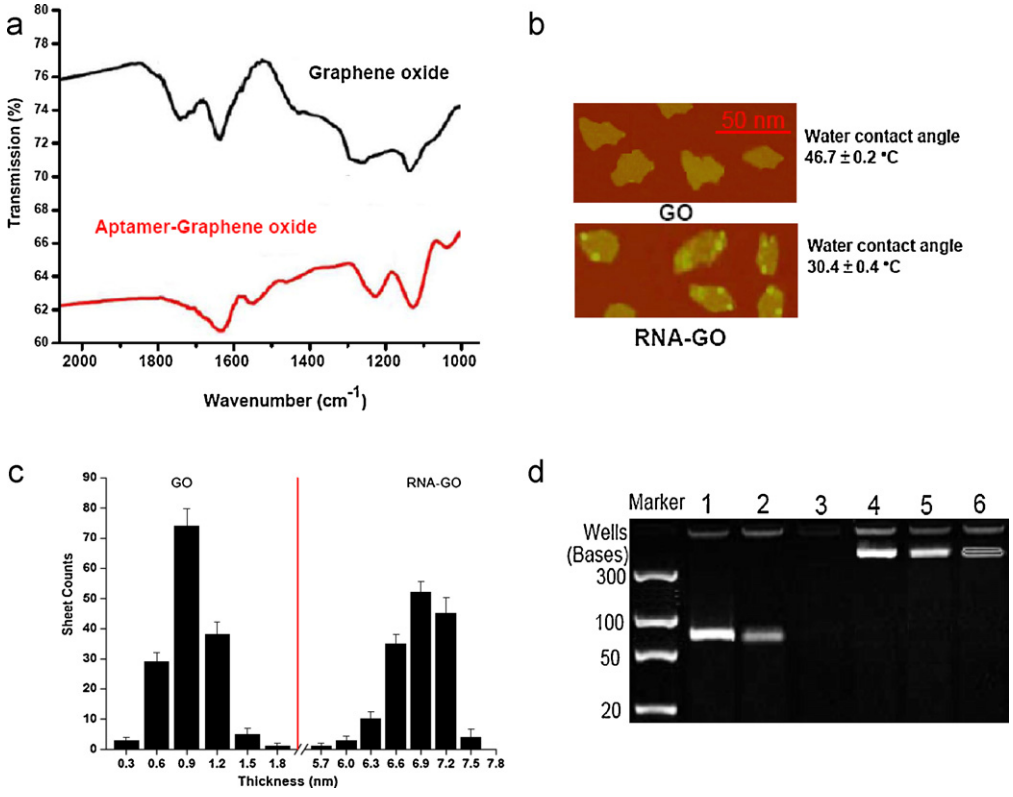

Fig. 2. Characteristics of RNA–graphene oxide nanosheets. (a) Fourier transform infrared spectra of graphene oxide and RNA–graphene oxide; (b) atomic force microscopy image of graphene oxide and RNA–graphene oxide; (c) statistics of graphene oxide and RNA–graphene oxide thickness measured by Atomic Force Microscopy; (d) agarose gel electrophoresis (lane 1 for bare RNA, lane 2 for bare RNA with nuclease for 6 h, lane 3 for bare RNA with nuclease for 12 h, lane 4 for RNA–GO, lane 5 for RNA–GO with nuclease for 6 h, and lane 6 for RNA–GO with nuclease for 12 h).

between the carboxyl groups on GO and the amine groups at the end of the modified RNA.

RNA is flexible, and its shape or size on solid surfaces is little known [9], especially on nanosheets. AFM was conducted to measure the size and thickness of GO and RNA–GO, as presented in Fig. 2b and c. Due to the presence of containing oxygen groups, GO formed a relative homogeneous dispersion [18]. To confirm and quantify the solubility of GO before and after immobilization of RNA, water contact angle was measured. The water contact angles of GO and RNA–GO were $46.7 \pm 0.2\,^{\circ}C$ and $30.1 \pm 0.4\,^{\circ}C$, respectively, which confirmed that RNA improved the solubility of GO. GO and RNA–GO were fairly polydispersed with a lateral dimension of approximately 20 nm. The average thickness of GO was 0.93 nm that was consistent with the thickness of single-layered GO [17,18]. The average thickness of RNA–GO was 7.86 nm, which was smaller than the value predicted by theory value (0.93 nm for single layer GO, 1.2 nm for the NH-C6 linker, and 0.43 nm for each base). The discrepancy implies that RNA is immobilized on the surface of GO nanosheets at an angle or a worm-like conformation.

The stability of RNA–GO against nuclease was investigated using agarose gel electrophoresis, as described in Fig. 2d. RNA and RNA–GO ($0.2\ mg\ mL^{-1}$) were incubated (v:v = 1:1) with RNase I ($0.01\ mg\ mL^{-1}$) at $25\,^{\circ}C$ for 6 h and 12 h. Agarose gel electrophoresis was conducted for 2 h at 100 V with ethidium bromide. To enhance the separation of RNA and RNA–GO, a low concentration (0.5%) of agarose was used in the work. Bare RNA was markedly digested with RNase I in 6 h (lane 2) and completely digested in 12 h (lane 3). In contrast, RNA–GO was digested slowly (lanes 5 and 6). These results demonstrate that RNA is protected from RNase I cleavage after RNA is covalently immobilized on GO. The similar protective effect was exhibited for the ssDNA adsorption on GO via noncovalent bond before ssDNA released from GO [21]. In this work, RNA covalently immobilized on GO should be more stable than that fixed by the noncovalent method. Probably, there are two paths of GO protecting RNA from nuclease. The steric hindrance could hinder the access of nuclease to RNA due to the covalent immobilization and noncovalent π–π stacking between RNA and GO. Moreover, GO may directly inactivate nuclease and then protect RNA. The interactions of RNA–GO with RNase need to be studied furthermore.

3.2. Adsorption kinetics and isotherms

Although adsorption kinetics is crucial to sorbents, the related information for aptamer is rare. Drinking water as medium was used for the experiment. The characteristics of drinking water were detected, including pH 7.6, hardness $CaCO_3$ $58\ mg\ L^{-1}$ and TOC $1.05\ mg\ L^{-1}$, respectively. The concentrations of Ca^{2+}, Mg^{2+}, K^{+}, Cl^{-}, and SO_4^{2-} were 32, 11, 8, 18 and 54 $mg\ L^{-1}$, respectively. The adsorption kinetic curves and related parameters for microcystin-LR are described in Fig. 3a. The adsorption equilibrium was achieved at approximately 100 min. The adsorption data were well-fitted using pseudo-second-order kinetics models with $R^2 > 0.99$. The results were consistent with the ssDNA adsorbing pharmaceuticals in drinking water [16]. The adsorption isotherms and related parameters are presented in Fig. 3b. The Langmuir model fit better than the Freundlich model, implying that the adsorption is homogenization. Based on Langmuir model, the maximum adsorption capacity of RNA–GO was 1,442 $ng\ mg^{-1}$, suggesting RNA–GO is suitable to remove the common contamination ($ng\ L^{-1}$) in drinking water. Freundlich constant n was found to be greater than 1, indicating a favorable condition for adsorption. The removal efficiency of toxins was calculated based on the adsorption isotherm curves. Approximately 95% of toxins were removed at the concentrations ranging from 50 to 2000 $ng\ L^{-1}$ that covered the reported toxin levels in drinking water [1]. The removal efficiency was comparable

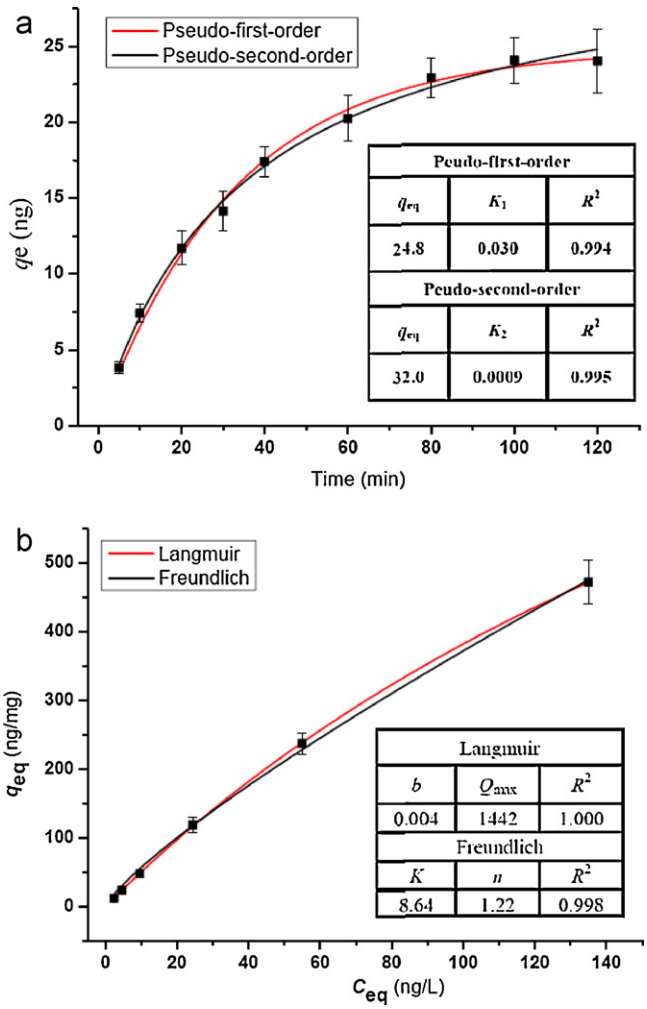

Fig. 3. Adsorption kinetics and isotherms of microcystin-LR on RNA–graphene oxide ($n = 3$).

with other chemical or biological methods [6,7], satisfied the maximum allowable concentration ($1\ \mu g\ L^{-1}$) prescribed by the world health organization (WHO) in human drinking water [8], and guaranteed the safety of purifying a lower contaminated concentration ($ng\ L^{-1}$).

3.3. Specific and competitive adsorption

To confirm the specific adsorption of trace peptide toxins on RNA–GO, a nonspecific test was conducted. Microcystin-RR, microcystin-LW and nodularin as cyclic pentapeptides have similar structures to microcystin-LR. The difference between the four peptide toxins is only one or two amino acids. The traditional chemical sorbents and antibodies with cross-reaction cannot isolate these microcystins very well [25]. In this work, more than 95% of microcystin-LR was absorbed by the smart RNA–GO. In contrast, less than 12% of the other three toxins (microcystin-RR, microcystin-LW and nodularin) were absorbed, as shown in Fig. 4. Compared with the smart RNA–GO, the random RNA–GO and bare GO bound to less than 3% of the all toxins. Hereby, there was a specific binding between RNA–GO and microcystin-LR. The specific binding from the free aptamer (ssDNA/RNA) was reported [12,26]. Moreover, this work proves that the immobilized aptamer (RNA) still has an intensive affinity to trace targets.

NOM widely exists in the actual environment and reduces the removal of pollutants [27]. However, the effects of NOM on aptamer

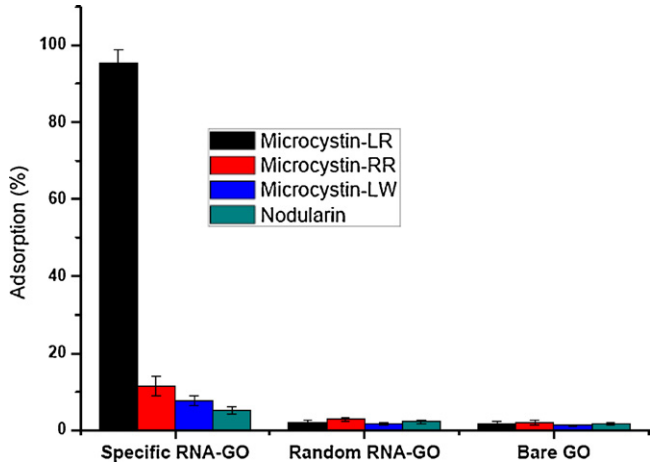

Fig. 4. Nonspecific (microcystin-RR, microcystin-LW and nodularin) and specific (microcystin-LR) adsorption using smart RNA–GO, random RNA–GO and bare GO in drinking water (spiked 500 ng L^{-1}, $n = 3$).

are unknown. SRHA was chosen as the model NOM in this work. The effects of NOM on the adsorption are described in Fig. 5. At a low NOM concentration (2 mg L^{-1}, higher than the common NOM concentration in drinking water), RNA–GO had more than 90% removal of microcystin-LR. The adsorption was reduced by 75% at a high NOM concentration (20 mg L^{-1}, close to the NOM concentration in river). Therefore, the adsorption of toxins on RNA–GO is influenced at a high concentration of NOM, but the effect is negligible for sources of drinking water with mild NOM.

3.4. Effects of pH, ionic strength and temperature

The activity of aptamer as the traditional nuclear acids can be influenced by pH, ionic strength and temperature. The effects of these physicochemical conditions on the adsorption of RNA–GO were tested, as shown in Fig. 5. The natural drinking water spiked 500 ng L^{-1} microcystin-LR was used as the control. The physicochemical properties of the natural drinking water were presented in Section 3.2. Compared with the control (pH 7.6), there was a slight reduction in the adsorption at pH 5 and 9. A very clear and highly effective temperature-operable adsorption was demonstrated by

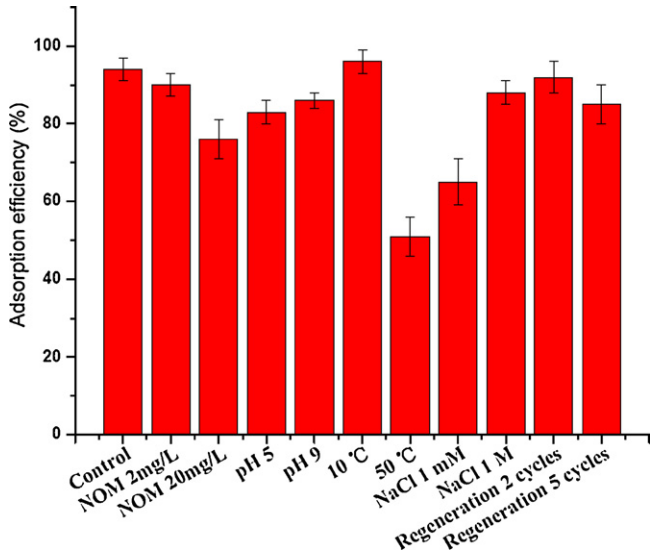

Fig. 5. Effects of physicochemical conditions of water on adsorption and regeneration of RNA–GO ($n = 3$).

monitoring the adsorption profile from 10 °C to 50 °C. Compared with the control (25 °C), the adsorption slightly increased at 10 °C, and dramatically decreased at 50 °C. This was consistent with the exothermic process of aptamer adsorption [16]. The removal of microcystin-LR was 88% at a high ionic strength (1 M NaCl). However, the removal was reduced to 65% at a low ionic strength (1 mM), suggesting that a certain ionic strength is preferred to adsorption. Interestingly, the tunable adsorption by temperature and ionic strength implies that the regeneration of RNA–GO is easy. The RNA–GO loaded microcystin-LR was regenerated in hot pure water at 50 °C for 10 min. The reusability of RNA–GO is presented in Fig. 5. The adsorption capacity reduced by less than 10% after 5 cycles.

3.5. Adsorption mechanisms

Carboxyl groups exists on the edge of GO, while small amount of epoxy and carbonyl groups are on GO [23]. RNA was successfully immobilized on GO via the reaction between the carboxyl group and the amino group, as shown in Figs. 1 and 2. The remaining epoxy and carbonyl groups could directly support RNA via electrostatic repulsion and steric hindrance. Therefore, the active sites of RNA on GO are independent, and the probability of one site being occupied is not dependent on the status of adjacent sites. The above theory was confirmed by Langmuir isotherm model of ssDNA/RNA in this and other work [28]. This special immobilization is beneficial in adsorbing targets and differs from other methods, such as fixed ssDNA/RNA on even silica or gold surfaces.

Microcystins with ketone, amino and aromatic groups can bind to GO by H-bonding, electrostatic interactions and π–π interactions. Van der Waals force probably occurs due to the large contact surface area of nanosheets. The adsorption capacity of GO is limited to less than 3%, as shown in Fig. 4, suggesting that the chemical interactions (H-bonding, electrostatic interactions and π–π interactions) are weaker than the affinity between RNA and toxins. RNA is unstable due to the intermolecular interactions and nuclease digestion [12], as described in Fig. 2d. The complex of RNA–GO obviates the defects of GO and bare RNA, and develops the merits of individuals.

It is well known that aptamers bind to targets by the changes in configuration [11]. Temperature, pH and ionic strength play important roles in the configurations of nuclear acids. The surface charges of microcystin-LR and RNA are negative at pH > 4 [29,30]. The increase of ionic strength or the decrease of pH is expected to reduce electrostatic repulsion between microcystin-LR and RNA, and then enhance microcystin-LR adsorption. RNA is prone to binding with targets in drinking water with medium ionic strength, and extreme low and high ionic concentrations reduce adsorption, due to the breakage of RNA configuration. The similar ionic effects occur between ssDNA and protein [26]. Generally, the pH for adsorption should be comparable with the condition (pH 7.4) in the selection buffer of aptamer [22,26,31]. However, the physicochemical conditions are various in actual sources of drinking water. The condition of pH 5–9 is acceptable to RNA–GO, as shown in Fig. 5. It is clear that RNA–GO prefers a low temperature, as indicated in Fig. 5. Probably, the high temperatures can destroy the conformation of aptamer. Furthermore, the adsorption of aptamer is an exothermic process [16].

3.6. Comparison with other sorbents

In the last twenty years, biological activity has been used to treat toxins in water [8]. It is notable that biotransformation from a less toxic to a more toxic toxin may occur [8]. Antibodies or enzymes have been widely applied to adsorb toxins. Compared with antibodies or enzymes, aptamer have its advantages, such as high affinity,

specificity, stability with targets and ease of preparation and modification at low cost [13]. Activated carbon is a low cost and stable sorbent [32], but the adsorption of activated carbon is nonspecific as other traditional chemical sorbents. Porous media (biochar, kaolin clay and ceramic particles) are frequently used as sorbents, and exhibit charming efficiency [33,34]. The regeneration and the influence from NOM are two big challenges to their application. Ozonation, ultraviolet radiation and other photocatalytic decomposition do not require continuous chemical addition to purify contaminated water, while they need an external energy source and produce the secondary contamination [35]. Nanomaterials are considered as potential sorbents due to their large surface areas and facile modification [4,36]. However, the aggregation, nonspecific adsorption and limited adsorption site inhibit the development of nanomaterials [4]. The smart RNA–GO nanosheets are a polydispersed, stable, reusable and molecular recognition, while their stability is inferior to other chemical sorbents.

4. Conclusions

Aptamer (RNA) was covalently immobilized on graphene oxide to form a polydispersed and stable nanosheet. RNA–graphene oxide can resist nuclease and natural organic matter, and specifically adsorb trace peptide toxins in drinking water. The adsorption data fit well with the pseudo-second-order kinetics and the Langmuir isotherm model. Extreme pH, temperature and ionic strength reduce the adsorption, as well as RNA–GO exhibits specific adsorption, high efficacy, and facile synthesis and regeneration. RNA–GO can be used to enrich and separate small molecules and biomacromolecules in purification of drinking water and preparation of environmental and biological samples.

Acknowledgment

This work was financially supported by the National Natural Science Foundation of China as a key project (21037002), the Shanghai Tongji Gao Tingyao Environmental Science & Technology Development Foundation (STGEF), the National Sciences and Engineering Research Council of Canada and the China Scholarship Council.

References

[1] S.M. Azevedo, W.W. Carmichael, E.M. Jochimsen, K.L. Rinehart, S. Lau, G.R. Shaw, G.K. Eaglesham, Human intoxication by microcystins during renal dialysis treatment in Caruaru-Brazil, Toxicology 181–182 (2002) 441–446.
[2] L.A. Lawton, H. Chambers, C. Edwards, A.A. Nwaopara, M. Healy, Rapid detection of microcystins in cells and water, Toxicon 55 (2010) 973–978.
[3] S. Dawan, P. Kanatharana, B. Wongkittisuksa, W. Limbut, A. Numnuam, C. Limsakul, P. Thavarungkul, Label-free capacitive immunosensors for ultra-trace detection based on the increase of immobilized antibodies on silver nanoparticles, Anal. Chim. Acta 699 (2011) 232–241.
[4] Q. Li, S. Mahendra, D.Y. Lyon, L. Brunet, M.V. Liga, D. Li, P.J. Alvarez, Antimicrobial nanomaterials for water disinfection and microbial control: potential applications and implications, Water Res. 42 (2008) 4591–4602.
[5] D. Li, D.Y. Lyon, Q. Li, P.J.J. Alvarez, Effect of natural organic matter on antibacterial activity of fullerene water suspension, Environ. Toxicol. Chem. 27 (2008) 1888–1894.
[6] L. Ho, A.L. Gaudieux, S. Fanok, G. Newcombe, A.R. Humpage, Bacterial degradation of microcystin toxins in drinking water eliminates their toxicity, Toxicon 50 (2007) 438–441.
[7] J. Li, K. Shimizu, M.K. Sakharkar, M. Utsumi, Z. Zhang, N. Sugiura, Comparative study for the effects of variable nutrient conditions on the biodegradation of microcystin-LR and concurrent dynamics in microcystin-degrading gene abundance, Bioresour. Technol. 102 (2011) 9509–9517.
[8] J.A. Westrick, D.C. Szlag, B.J. Southwell, J. Sinclair, A review of cyanobacteria and cyanotoxins removal/inactivation in drinking water treatment, Anal. Bioanal. Chem. 397 (2010) 1705–1714.
[9] L. Moiseev, M.S. Unlü, A.K. Swan, B.B. Goldberg, C.R. Cantor, DNA conformation on surfaces measured by fluorescence self-interference, Proc. Natl. Acad. Sci. U.S.A. 103 (2006) 2623–2628.
[10] T. Hermann, D.J. Patel, Adaptive recognition by nucleic acid aptamers, Science 287 (2000) 820–825.
[11] J.L. Vinkenborg, N. Karnowski, M. Famulok, Aptamers for allosteric regulation, Nat. Chem. Biol. 7 (2011) 519–527.
[12] V.J. Ruigrok, M. Levisson, M.H. Eppink, H. Smidt, J. van der Oost, Alternative affinity tools: more attractive than antibodies? Biochem. J. 436 (2011) 1–13.
[13] A.C. Yan, M. Levy, Aptamers and aptamer targeted delivery, RNA Biol. 6 (2006) 316–320.
[14] M. Kim, H.J. Um, S. Bang, S.H. Lee, S.J. Oh, J.H. Han, K.W. Kim, J. Min, Y.H. Kim, Arsenic removal from Vietnamese groundwater using the arsenic-binding DNA aptamer, Environ. Sci. Technol. 43 (2009) 9335–9340.
[15] N. Dave, M.Y. Chan, P.J.J. Huang, B.D. Smith, J.W. Liu, Regenerable DNA-functionalized hydrogels for ultrasensitive, instrument-free mercury (II) detection and removal in water, J. Am. Chem. Soc. 132 (2010) 12668–12673.
[16] X. Hu, L. Mu, Q. Zhou, J. Wen, J. Pawliszyn, ssDNA aptamer-based column for simultaneous removal of nanogram per liter level of illicit and analgesic pharmaceuticals in drinking water, Environ. Sci. Technol. 45 (2011) 4890–4895.
[17] K.S. Novoselov, A.K. Geim, S.V. Morozov, D. Jiang, Y. Zhang, S.V. Dubonos, I.V. Grigorieva, A.A. Firsov, Electric field effect in atomically thin carbon films, Science 306 (2004) 666–669.
[18] Y. Zhu, S. Murali, W. Cai, X. Li, J.W. Suk, J.R. Potts, R.S. Ruoff, Graphene and graphene oxide: synthesis, properties, and applications, Adv. Mater. 22 (2010) 3906–3924.
[19] T.S. Sreeprasad, S.M. Maliyekkal, K.P. Lisha, T. Pradeep, Reduced graphene oxide-metal/metal oxide composites: facile synthesis and application in water purification, J. Hazard. Mater. 186 (2011) 921–931.
[20] K. Zhang, V. Dwivedi, C. Chi, J. Wu, Graphene oxide/ferric hydroxide composites for efficient arsenate removal from drinking water, J. Hazard. Mater. 182 (2010) 162–168.
[21] Y. Wang, Z. Li, D. Hu, C.T. Lin, J. Li, Y. Lin, Aptamer/graphene oxide nanocomplex for in situ molecular probing in living cells, J. Am. Chem. Soc. 132 (2010) 9274–9276.
[22] K.D. Gu, M. Famulok, In vitro selection of specific aptamers against microcystin-LR, Chin. J. Prev. Med. 38 (2004) 369–373.
[23] X.F. Gao, J. Jang, S. Nagase, Hydrazine and thermal reduction of graphene oxide: reaction mechanisms, product structures, and reaction design, J. Phys. Chem. C 114 (2010) 832–842.
[24] X. Sun, Z. Liu, K. Welsher, J.T. Robinson, A. Goodwin, S. Zaric, H. Dai, Nano-graphene oxide for cellular imaging and drug delivery, Nano Res. 1 (2008) 203–212.
[25] R. Aranda-Rodriguez, C. Kubwabo, F.M. Benoit, Extraction of 15 microcystins and nodularin using immunoaffinity columns, Toxicon 42 (2003) 587–599.
[26] T. Hianik, V. Ostatná, M. Sonlajtnerova, I. Grman, Influence of ionic strength, pH and aptamer configuration for binding affinity to thrombin, Bioelectrochemistry 70 (2007) 127–133.
[27] P.A. Neale, A. Antony, W. Gernjak, G. Leslie, B.I. Escher, Natural versus wastewater derived dissolved organic carbon: implications for the environmental fate of organic micropollutants, Water Res. 45 (2011) 4227–4237.
[28] P. Calik, O. Balci, T.H. Ozdamar, Human growth hormone-specific aptamer identification using improved oligonucleotide ligand evolution method, Protein Expr. Purif. 69 (2010) 21–28.
[29] P.S. Vesterkvist, J.A. Meriluoto, Interaction between microcystins of different hydrophobicities and lipid monolayers, Toxicon 41 (2003) 349–355.
[30] M.G. Antoniou, A.A. de la Cruz, D.D. Dionysiou, Cyanotoxins: new generation of water contaminants, J. Environ. Eng. 131 (2005) 1239–1243.
[31] D.M. Kolpashchikov, Binary probes for nucleic acid analysis, Chem. Rev. 110 (2010) 4709–4723.
[32] D. Cook, G. Newcombe, Comparison and modeling of the adsorption of two microcystin analogues onto powdered activated carbon, Environ. Technol. 29 (2008) 525–534.
[33] Y. Qiu, Z. Zheng, Z. Zhou, G.D. Sheng, Effectiveness and mechanisms of dye adsorption on a straw-based biochar, Bioresour. Technol. 100 (2009) 5348–5351.
[34] V. Gitis, C. Dlugy, J. Gun, O. Lev, Studies of inactivation, retardation and accumulation of viruses in porous media by a combination of dye labeled and native bacteriophage probes, J. Contam. Hydrol. 124 (2011) 43–49.
[35] H. Schaar, M. Clara, O. Gans, N. Kreuzinger, Micropollutant removal during biological wastewater treatment and a subsequent ozonation step, Environ. Pollut. 158 (2010) 1399–1404.
[36] M.B. Dixon, C. Falconet, L. Ho, C.W. Chow, B.K. O'Neill, G. Newcombe, Removal of cyanobacterial metabolites by nanofiltration from two treated waters, J. Hazard. Mater. 188 (2011) 288–295.